catalysts

MDPI

Article

Porosity Design of Shaped Zeolites for Improved Catalyst Lifetime in the Methanol-to-Hydrocarbons Reaction

Rogéria Bingre [1], Renna Li [2], Qiang Wang [2], Patrick Nguyen [3], Thomas Onfroy [4] and Benoît Louis [1,*]

1 ICPEES—Institut de Chimie et Procédés pour l'Energie, l'Environnement et la Santé, Energy and Fuels for a Sustainable Environment Team, UMR 7515 CNRS—Université de Strasbourg—ECPM, 25 rue Becquerel, F-67087 Strasbourg CEDEX 2, France; rpmartins@etu.unistra.fr

2 EFN—Environmental Functional Nanomaterials Lab, College of Environmental Science and Engineering, Beijing Forestry University, P.O. Box 60, 35 Qinghua East Road, Haidian District, Beijing 100083, China; lrenna@bjfu.edu.cn (R.L.); qiangwang@bjfu.edu.cn (Q.W.)

3 Saint-Gobain C.R.E.E., 550 Avenue Alphoense Jauffret, BP 224, 84306 Cavaillon CEDEX, France; Patrick.Nguyen@saint-gobain.com

4 Sorbonne Université, CNRS, Laboratoire de Réactivité de Surface (LRS), F-75005 Paris, France; thomas.onfroy@upmc.fr

* Correspondence: blouis@unistra.fr; Tel.: +33-368-852-766

Received: 24 May 2019; Accepted: 16 June 2019; Published: 18 June 2019

Abstract: Additional porosity, such as meso- and macropores, was introduced in zeolite extrudates with the intention intuit of improving the effective diffusivity of the catalysts. The samples were characterized in depth by nitrogen adsorption-desorption, mercury intrusion porosimetry, ammonia temperature programmed desorption and adsorption of pyridine followed by infrared spectroscopy. The results revealed no significant change in the acidity but an increase of the pore volume. According to significant improvement in the effective diffusivity, the samples were tested in the methanol-to-hydrocarbons reaction. The catalytic stability was greatly enhanced with an increase in the pore volume, demonstrating a relation between effective diffusivity and resistance to deactivation by coke formation. Further experiments also revealed a higher toluene adsorption capacity and a raise in the breakthrough time over the most porous samples due to better accessibility of toluene molecules into the active sites of the zeolite.

Keywords: zeolite extrudates; porosity; effective diffusivity; methanol-to-hydrocarbons; catalyst lifetime

1. Introduction

Since their discovery, zeolites have been widely used in industrial applications [1,2]. Their unique properties, such as crystalline structure, shape-selectivity, and strong acidity render them extremely useful materials for catalysis. In principle, zeolites are synthesized in the form of a powder with poor mechanical strength that can induce damage or degradation of the catalyst, thus leading to fines at the industrial reactor bottom. In this way, these catalysts are often shaped into centimeter-sized bodies, by addition of a non-zeolitic binder, to be abrasion and fracture resistant during loading and transport.

The presence of those binders may affect the zeolite performance [3–12]. For instance, the binder can block the pores of the zeolite, thus diminishing the rate of mass transfer within the porosity. Associating this feature with the known slow molecular diffusion in the zeolite structure itself [13–17], several strategies for improving the molecular transport in technical zeolite bodies have been developed, such as (i) introduction of hierarchical porosity within the zeolite structure; (ii) coating of zeolite crystals onto monoliths; (iii) binder-free strategies. The first approach has been widely investigated, with results showing improvements of conversion, selectivity and catalyst lifetime in many important

acid-catalyzed reactions [18–25]. However, there is a lack of understanding of the real influence of the binder in hierarchical zeolites, despite important contributions from Pérez-Ramirez's group [9,26–28]. In processes where the pressure drop plays a crucial role, structured catalysts remain the best strategy to overcome mass transfer limitations [20]. Several approaches to prepare zeolite macrostructures have been reported as the coating of zeolite onto ceramic/metallic structures [29–36]. Besides, several researchers also succeeded in avoiding the use of binders to overcome those issues encountered during the shaping process. They are based in the compression of zeolite powders, the use of removable matrix, the hydrothermal transformation of dense aluminosilicate gels, and the use of pre-shaped amorphous materials [37–46]. However, these methodologies remain at the laboratory scale due to expensive or unpractical techniques and materials, with little prediction of any industrial use in the near future.

In this article, we propose a strategy to improve the mass transfer within zeolite bodies, by means of introduction of additional porosity in the alumina binder used during the conventional extrusion process. In our previous study [47], an improvement of effective diffusivity of toluene attributed to additional meso- or macropores was assessed. Herein, an in-depth characterization of the samples is presented, along with toluene adsorption under plug-flow conditions and catalytic tests in order to enlighten the influence of the effective diffusivity on the conversion, selectivity, and catalyst lifetime.

2. Results and Discussion

2.1. Structural Properties

Table 1 summarizes the textural properties obtained by N_2 isotherms and mercury intrusion porosimetry (MIP), namely, specific surface area, S_{BET}, micropore volume, V_μ, and pore volume at $P/P^\circ = 0.95$, V_p, total intrusion volume, $V_{total\ intrusion}$, and porosity, respectively.

Table 1. Summary of the structural properties of as-prepared samples.

Sample	S_{BET} (m^2/g)	V_μ (cm^3/g)	V_p (cm^3/g)	$V_{total\ intrusion}$ (mL/g)	Porosity (%)
Boeh_ext	237	-	0.36	-	-
CBV3020E	369	0.11	0.23	-	-
Catal_ref	337	0.09	0.25	0.43	43
Catal_5PA1	347	0.09	0.25	0.58	52
Catal_10PA1	344	0.09	0.25	0.65	54
Catal_20PA1	348	0.09	0.25	0.78	58
Catal_PA2	348	0.09	0.32	0.81	60

It is obvious that extruded boehmite (boeh_ext) exhibits lower S_{BET} than pristine commercial zeolite (CBV3020E) and mesopores of 4.5 nm obtained by BJH method (Figure S1). This result is in line with former studies on γ-alumina [48–52]. Concerning shaped ZSM-5 (Catal_ref), both S_{BET} (Table 1) and micropore volume of the catalytic bodies diminished upon extrusion, probably associated with the binder presence [10]. BJH pore size distribution profiles are given in Figure 1. All samples exhibit at least two peaks in the range of 3.5 to 6.5 nm characteristic of crystalline voids formed between zeolite crystals. In addition, Catal_PA2 presents extra-mesopores centered at 12 nm, whereas Catal_10PA1 exhibited macropores ranging from 400 to 1000 nm as determined by MIP. This can be attributed to the pore former agent added during the extrusion step, which upon calcination was burned off, leaving voids in the catalyst body. It is worthy to mention that an increase in the quantities of PA1 (Catal_5PA1, Catal_10PA1, and Catal_20PA1, respectively) led to an increase of the macropores presence (Figure S2). This result is in agreement with the higher intrusion volume reported in Table 1 and the pore profile of the samples in Figure S3. Regarding the Catal_PA2 sample, macropores in the 10–1000 μm range were evidenced by MIP. However, the latter macropores are probably due to cracks present in the technical body rather to macropores formed by the presence of pore former agents. Indeed, microprobe SEM

analysis (Figure 2) reveals the presence of macropores in Catal_10PA1 that are not present in Catal_ref, as well as the presence of cracks in Catal_PA2.

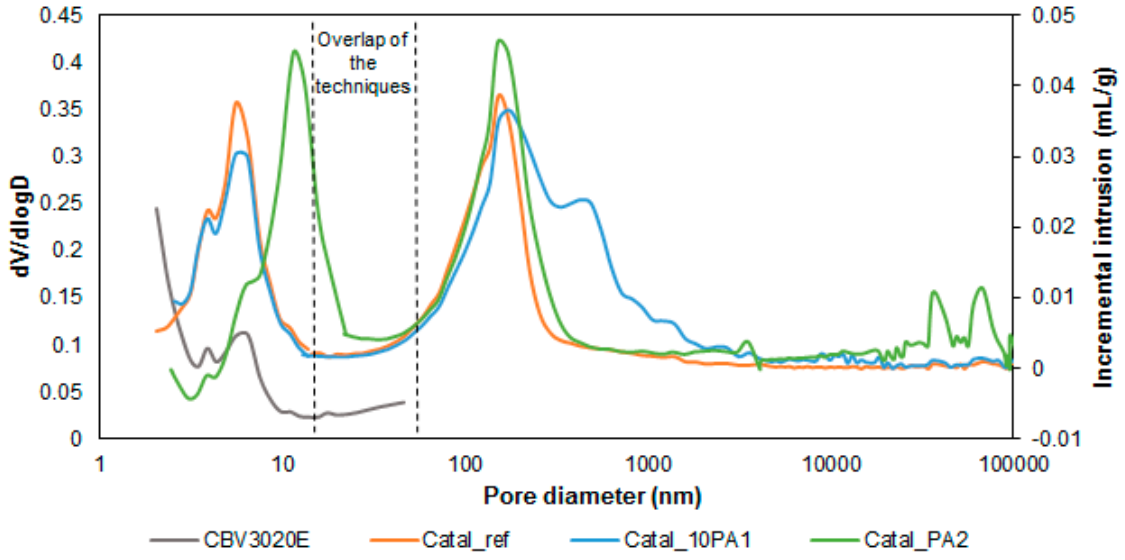

Figure 1. Pore size distribution profiles of the samples obtained by N_2 adsorption isotherms (from 1 to 50 nm) and mercury intrusion porosimetry (MIP, from 20 to 100,000 nm).

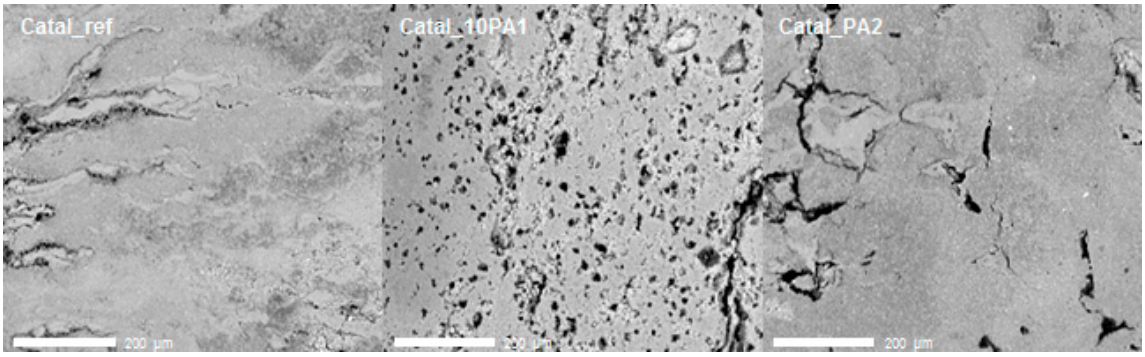

Figure 2. Microprobe SEM image of Catal_ref, Catal_10PA1, and Catal_PA2 revealing the macropores (black mark) formed by the presence of the pore former agent during the extrusion process.

NH_3 thermal desorption analysis (Figure 3) shows two peaks at 220 and 500 °C, that can be associated to two types of acid sites: weak and strong, respectively. Considering the peak at higher temperatures, the concentration of acid sites could be estimated as 249 µmol/g for CBV3020E, 223 µmol/g for Catal_ref, 250 µmol/g for Catal_10PA1, and 218 µmol/g for Catal_PA2. The acidity profile of boeh_ext revealed the presence of mainly weak acid sites, being located at 220 °C. This shows that the presence of the binder in the zeolite extrudates did not induce additional acidity, as the total acidity of the extrudates corresponds approximately to 80% of the acidity of CBV3020E (quantity of zeolite used in the extrusion process). Moreover, it is noteworthy that no shift of the peak at higher temperatures could be evidenced among the different samples. In contrast to previous studies showing a higher desorption temperature, hence a higher acid strength [53,54], the strategy presented herein did not induce changes in the acidity of the materials. This is extremely important for catalytic purposes.

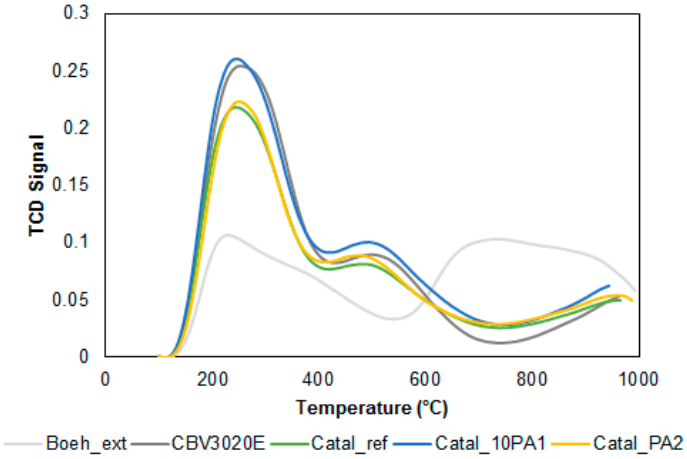

Figure 3. Temperature programmed desorption of NH_3 (NH_3-TPD) profiles of as-synthesized catalysts.

The adsorption of pyridine followed by FTIR allowed the determination of the total quantity of BrØnsted acid sites, being 350 µmol/g for CBV3020E, 300 µmol/g for Catal_ref, 240 µmol/g for Catal_10PA1, and 310 µmol/g for Catal_PA2 (Figure S4). The results deviate only slightly from the ones of NH_3-TPD, being explained by different methods used for both techniques. In general, one may admit low changes in the acidity of the samples, confirming aforementioned observations.

2.2. *Catalytic Activity*

The performance of zeolite extrudates was evaluated in the conversion of methanol to hydrocarbons. The catalyst lifetime could be estimated as the time for which the conversion of oxygenates (methanol and dimethyl ether) decreased below 90%, represented in Figure 4. The selectivity in C_2-C_4 olefins and C_{5+} products after 1 h of reaction are summarized in Table 2.

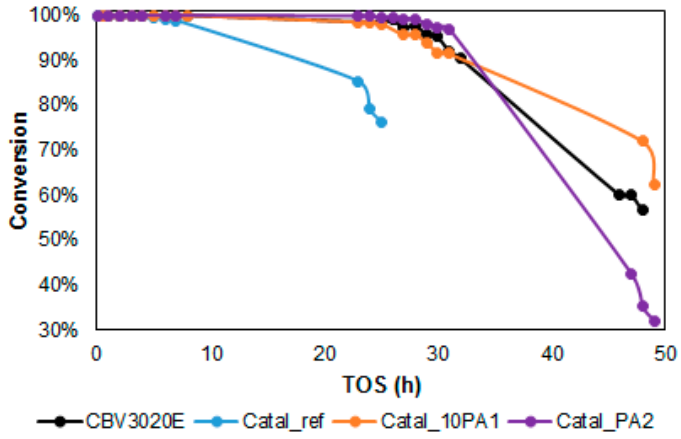

Figure 4. Profiles of the different catalysts' lifetimes.

The extrudate commercial zeolite (Catal_ref) exhibited a lifetime almost half of the pristine powder CBV3020E catalyst, and only minor differences in selectivity were noted. This may prove former observations concerning the hampering effects of binders on the catalytic activity, possibly caused by a decrease of the effective diffusivity through the catalyst body. Previous reports suggested that the presence of the binder may partially block the pores of the zeolite, thus hindering the diffusion of the molecules to and from the active sites. In contrast, the samples where meso- and macropores were introduced (Catal_PA1 and Catal_PA2), present a substantial improvement in the catalyst lifetime, reaching almost the same behavior as the commercial powder. We recently reported that the presence of hierarchical porosity in the zeolite extrudates allowed better mass transport, verified by three

different techniques of effective diffusion measurements [47]. The catalytic activity of the samples in the methanol-to-hydrocarbons (MTH) reaction seems therefore directly related to the effective diffusivity, as its increase led to a superior catalyst lifetime.

Table 2. Selectivity of the samples in methanol-to-hydrocarbons (MTH) of C_3H_6 (propylene), C_2-C_4 (olefins with two to four carbons) and C_{5+} (hydrocarbons with more than five carbons including aromatics).

Sample	S_{C3H6} (%)	S_{C2-C4} (%)	S_{C5+} (%)
CBV3020E	25	65	33
Catal_ref	27	70	29
Catal_10PA1	26	68	30
Catal_PA2	24	64	33

Besides, it is known that BrØnsted acid sites play a key role in the conversion of methanol, and it was observed that the selectivity of all samples remained unchanged in comparison with the commercial zeolite (Table 2). This may be due to the fact that the acidity was not altered during the extrusion process as showed in the previous section. Moreover, our strategy was aimed at the introduction of additional porosity in the binder only, preserving the zeolite structure intact. Since alumina did not exhibit significant activity in the methanol conversion reaction (Figure S5), the differences may only be attributed to the improvement of the effective diffusivity in the overall catalyst body.

To further analyze the impact of macropores presence in zeolite extrudates, the samples prepared with different quantities of the pore former agent PA1 were also tested. An increase in the catalyst lifetime is clearly evidenced when the quantity of PA1 was enhanced (Figure 5). Although diffusion measurements were not performed, the sole difference between these three samples remains the quantity of macropores formed (Table 1), which led to an improvement of the effective diffusivity in comparison with Catal_ref. Furthermore, the coking behavior was analyzed by TGA (Figure 6) showing larger quantities of the latter in samples which exhibited superior lifetime. It seems that the macropores may have the ability to "trap" coke molecules, hence, to keep the acid sites on the zeolite internal surface "free" for performing the reaction, allowing a full conversion of oxygenates (methanol and dimethylether) over a longer time (Figure 5). This agrees with the results obtained for the samples Catal_XPA1, however this is not observed in Catal_PA2 that exhibited lower coke amount than Catal_ref (the sample with lower lifetime). This may be attributed to the presence of both mesopores and cracks, that may induce a network of pores in the binder allowing the exit of coke precursors instead of trapping them as suggested for the remaining samples.

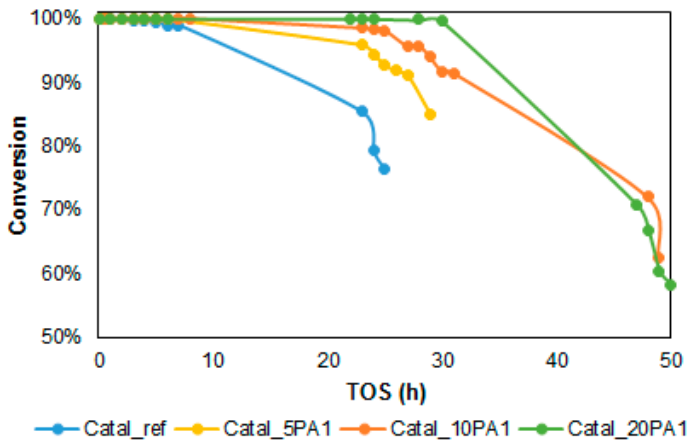

Figure 5. Comparison of the lifetime of as-prepared samples with different quantities of PA1.

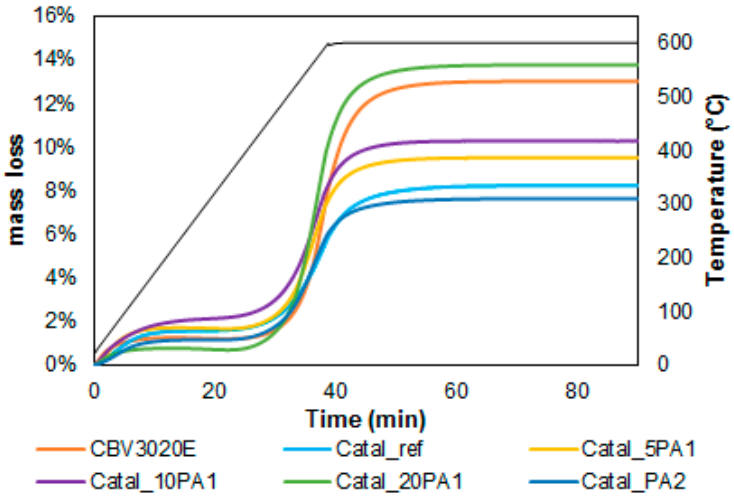

Figure 6. Percentage of mass lost during the increase of the temperature determined by TGA under air.

Lastly, the samples were subjected to toluene adsorption under dry conditions (Figure 7). The capacities of toluene adsorption of the samples were found to be 15.5, 68.0, 63.4, 70.0, and 62.3 mg/g for boeh_ext, CBV3020E, Catal_ref, Catal_10PA1, and Catal_PA2, respectively. Some differences between the samples were observed, the most notable being the increase in the breakthrough time. The latter is defined as the time that the adsorbent is capable of adsorbing all the toluene in the stream, and the introduction of macropores allowed an increase from 8 to 30 min (Catal_ref and Catal_PA1, respectively). This may suggest that the presence of *highways* in the catalytic technical body facilitates the diffusion of toluene molecules to and from the active sites within the zeolite where adsorption takes place. This is also somehow applied to Catal_PA2, although no significant improvement in the breakthrough time (8 min) could be observed. However, the latter sample is able to reach the saturation faster than Catal_ref without extensive loss in its adsorption capacity which suggests an improvement in the accessibility to the active sites.

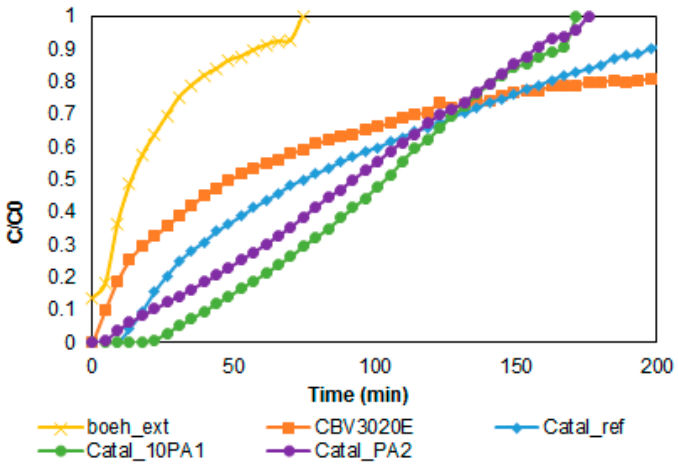

Figure 7. Adsorption breakthrough curves of toluene (400 ppm in 100 mL/min Ar flow).

3. Experimental

3.1. Catalysts and Materials

The technical bodies were obtained by extrusion of commercial ZSM-5 zeolite (CBV3020E, Zeolyst) with boehmite (SASOL Disperal P2) in a mass ratio of 4:1, respectively. Two different pore former agents, consisting of surfactants with a long organic chain, were added to the mixture to introduce meso-

or macropores in the binder, being the samples labelled Catal_PAX (being X a number corresponding to different pore former agents). Some samples were prepared with different quantities of PA1, specifically 5, 10, and 20 wt%, and named Catal_5PA1, Catal_10PA1, and Catal_20PA1, respectively, while Catal_PA2 was prepared with 10 wt% of pore former agent PA2. Pure boehmite was extruded (boeh_ext) and a reference sample without any addition of pore former agent was also prepared (Catal_ref). The mixture of solids was wet with 40% (solids base) of an aqueous solution of HNO_3 4%. The paste formed was extruded in a Walnut Hollow Clay Extruder. All the samples were calcined in a furnace at 600 °C for 4 h with a heating ramp of 1 °C/min, and further ground and sieved to obtain an equivalent diameter of 2.9 mm.

3.2. Characterization

Focused ion beam scanning electron microscopy (SEM) micrographs of resin-embedded extrudates were acquired on a microprobe JEOL FEG JXA8530F with spectrometers WDS and EDS JEOL. The samples were coated with Au for 60 s.

The textural properties of the extrudates involving the Brunauer–Emmett–Teller surface area (S_{BET}) were evaluated from classical nitrogen physical adsorption-desorption isotherms measured at −196 °C by means of ASAP2020M equipment (Micromeritics). In addition, mercury intrusion porosimetry (MIP) was performed in a Micromeritics AutoPore IV 9510 operated in the pressure range from vacuum to 414 MPa. Samples in their extruded forms were degassed in situ prior to measurement. A contact angle of 140° for mercury and a pressure equilibration time of 10 s were used. The total intrusion volume was obtained by the total quantity introduced until 414 MPa and the pore size distribution was determined by application of the Washburn equation.

Temperature programmed desorption of NH_3 (NH_3-TPD) of the extrudates was carried out in an AutoChem II from Micromeritics equipped with a thermal conductivity detector (TCD). The samples were pre-treated at 500°C in flowing He for 1 h. NH_3 was adsorbed until saturation under a continuous flow at 100 °C. The desorption was performed by increasing the temperature up to 1000 °C with a heating ramp of 20 °C/min. During this process, the concentration of the desorbed species was monitored.

The acidic properties of the samples were also evaluated by adsorption of pyridine followed by infrared spectroscopy. Prior to analysis, samples were pressed at ~1 tons.cm^{-2} into thin wafers of ca. 10 mg.cm^{-2} and placed inside the IR cell. Before pyridine adsorption/desorption experiments, the wafers were calcined in static conditions at 400 °C for 1 h in O_2 (15 kPa) and then outgassed under secondary vacuum at 400 °C for 1 h. These wafers were contacted at 150 °C with gaseous pyridine (67 Pa) via a separate cell containing liquid pyridine. The spectra were then recorded following desorption from 150 and 300 °C with a Bruker Vector 22 spectrometer (resolution 4 cm^{-1}, 64 scans). The reported spectra were obtained after subtraction of the spectrum recorded before pyridine adsorption. The amount of Brønsted and Lewis acidic sites titrated by pyridine was obtained using a molar absorption coefficient value of ε = 1.14 cm.µmol^{-1} for the ν_{19b} vibration of protonated pyridine (Py-H$^+$) at ~1545 cm^{-1} and of ε = 1.76 cm.µmol^{-1} for the ν_{19b} vibration of coordinated pyridine (Py-L) at ~1455 cm^{-1} [55,56].

Coke analysis of the extrudates was performed in TGA Q5000 equipment by placing the sample in the sample holder and raising the temperature at 15 °C/min from room temperature to 600 °C, while holding it for 1 h under air flow. The mass of the sample was recorded during the whole process.

3.3. Methanol-to-Hydrocarbons (MTH) Reaction

Prior to use, catalysts were calcined at 550 °C for 1 h under argon flow. A total of 1.5 g of zeolite bodies with 2.9 mm of equivalent diameter were placed in a tubular quartz reactor and packed between two quartz wool plugs. CBV3020E was tested in its powder form with particle diameter around 200 µm. A constant argon flow was fed through a methanol saturator, heated to 45 °C by an oil bath, to achieve WHSV = 2.0 $g_{MEOH}/g_{cat}.h^{-1}$. The reactant was subsequently fed to the reactor containing the catalyst at 450 °C. The products at the outlet were analyzed by GC equipped with a 50 m capillary column

(PONA) and a flame ionization detector (FID). The conversion of the samples was expressed in terms of methanol and dimethyl ether (DME considered as a reactant) consumption, calculated from the difference between inlet and outlet concentrations. The selectivity was given by the mole ratio of each product referred to the moles of converted methanol and DME.

3.4. Toluene Adsorption

Catalysts were calcined at 600 °C for 1 h in static air, prior to use. Toluene adsorption in volatile organic compounds (VOC) removal conditions was performed in a fixed bed reactor at 40 °C. The flow consisted in 400 ppm of toluene in the presence of O_2 and Argon in a total of 100 mL/min. The gas outlet was analyzed by GC equipped with a flame ionization detector (FID) and a column Agilent 125-7062 DB-Wax 60 m × 530 µm × 1 µm.

4. Conclusions

Through systematic comparison of conventional extrudate zeolites and extrudate zeolites with meso- and/or macropores, we demonstrated a strategy to improve the catalyst lifetime in the methanol to hydrocarbons reaction. The introduction of additional porosity by means of pore former agents during the extrusion process, enhanced the total macropore volume of the samples without significantly modifying their acidity, which plays a major role in the performance of zeolites in acid-catalyzed reactions.

By changing the quantity of pore former agent, the macropore volume was also increased, leading to an improved catalyst lifetime. As it was assessed before, the creation of additional porosity led to higher effective diffusivity. This parameter can therefore be directly related to the catalyst performance. Coke analysis showed larger quantities in the samples with higher catalytic stability that may have been kept in the macropores of the binder, leaving the active sites in operation for a longer time. Moreover, the samples were also tested in toluene adsorption, and once again the presence of macropores had a positive impact on the breakthrough time.

Supplementary Materials: The following are available online at http://www.mdpi.com/2073-4344/9/6/545/s1, Figure S1: Pore size distribution of boeh_ext obtained by BJH method, Figure S2: SEM images of the samples with different quantities of PA1: (**a**) Catal_5PA1; (**b**) Catal_10PA1; (**c**) Catal_20PA1, Figure S3: Pore profile of the samples with different quantities of PA1 obtained by mercury intrusion porosimetry, Figure S4: Spectra of pyridine adsorption followed by FTIR after desorption at 150 °C, Figure S5: Catalytic activity of boeh_ext: Conversion of methanol and selectivity in methane and dimethyl ether.

Author Contributions: Investigation, R.B., R.L. and T.O.; Data curation, R.B., P.N. and B.L.; Writing—Original Draft Preparation, R.B.; Writing—Review and Editing, Q.W., T.O. and B.L., Funding Acquisition, P.N.

Acknowledgments: This work was supported by Grand-Est Region and Saint-Gobain/Norpro. The authors are grateful to the French Ministry of Foreign Affairs and the Chinese Science Council for financially supporting the PHC Cai Yuanpei (no. 38892 SL).

Conflicts of Interest: The authors declare no conflict of interest.

References

1. Corma, A. From Microporous to Mesoporous Molecular Sieve Materials and Their Use in Catalysis. *Chem. Rev.* **1997**, *97*, 2373–2419. [CrossRef] [PubMed]
2. Tanabe, K.; Hölderich, W.F. Industrial Application of Solid Acid-Base Catalysts. *Appl. Catal. A* **1999**, *181*, 399–434. [CrossRef]
3. Uguina, M.A.; Sotelo, J.L.; Serrano, D.P. Toluene Disproportionation over ZSM-5 Zeolite. Effects of Crystal Size, Silicon-to-Aluminum Ratio, Activation Method and Pelletization. *Appl. Catal.* **1991**, *76*, 183–198. [CrossRef]
4. Martin, A.; Berndt, H.; Lohse, U.; Wolf, U. Effect of Si: Al Ratio and Type of Binder on the Catalytic Properties of HZSM-5 Catalysts. *J. Chem. Soc. Faraday Trans.* **1993**, *89*, 1277–1282. [CrossRef]
5. Romero, M.D.; Calles, J.A.; Rodríguez, A.; De Lucas, A. Acidity Modification during the Agglomeration of ZSM-5 with Montmorillonite. *Microporous Mater.* **1997**, *9*, 221–228. [CrossRef]

6. Freiding, J.; Patcas, F.C.; Kraushaar-Czarnetzki, B. Extrusion of Zeolites: Properties of Catalysts with a Novel Aluminium Phosphate Sintermatrix. *Appl. Catal. A* **2007**, *328*, 210–218. [CrossRef]
7. Lee, K.Y.; Lee, H.K.; Ihm, S.K. Influence of Catalyst Binders on the Acidity and Catalytic Performance of HZSM-5 Zeolites for Methanol-to-Propylene (MTP) Process: Single and Binary Binder System. *Top. Catal.* **2010**, *53*, 247–253. [CrossRef]
8. Freiding, J.; Kraushaar-Czarnetzki, B. Novel Extruded Fixed-Bed MTO Catalysts with High Olefin Selectivity and High Resistance against Coke Deactivation. *Appl. Catal. A* **2011**, *391*, 254–260. [CrossRef]
9. Mitchell, S.; Michels, N.L.; Kunze, K.; Pérez-Ramírez, J. Visualization of Hierarchically Structured Zeolite Bodies from Macro to Nano Length Scales. *Nat. Chem.* **2012**, *4*, 825–831. [CrossRef] [PubMed]
10. Bingre, R.; Louis, B.; Nguyen, P. An Overview on Zeolite Shaping Technology and Solutions to Overcome Diffusion Limitations. *Catalysts* **2018**, *8*, 163. [CrossRef]
11. Verkleij, S.P.; Whiting, G.T.; Esclapez, S.P.; Mertens, M.M.; Bons, A.J.; Burgers, M.; Weckhuysen, B.M. Operando Micro-Spectroscopy on ZSM-5 Containing Extrudates during the Oligomerization of 1-Hexene. *Catal. Sci. Technol.* **2018**, *8*, 2175–2185. [CrossRef]
12. Hernando, H.; Ochoa-Hernández, C.; Shamzhy, M.; Moreno, I.; Fermoso, J.; Pizarro, P.; Coronado, J.M.; Čejka, J.; Serrano, D.P. The Crucial Role of Clay Binders in the Performance of ZSM-5 Based Materials for Biomass Catalytic Pyrolysis. *Catal. Sci. Technol.* **2019**, *9*, 789–802. [CrossRef]
13. Chaikittisilp, W.; Suzuki, Y.; Mukti, R.R.; Suzuki, T.; Sugita, K.; Itabashi, K.; Shimojima, A.; Okubo, T. Formation of Hierarchically Organized Zeolites by Sequential Intergrowth. *Angew. Chem. Int. Ed.* **2013**, *52*, 3355–3359. [CrossRef] [PubMed]
14. White, R.J.; Fischer, A.; Goebel, C.; Thomas, A. A Sustainable Template for Mesoporous Zeolite Synthesis. *J. Am. Chem. Soc.* **2014**, *136*, 2715–2718. [CrossRef] [PubMed]
15. Verboekend, D.; Pérez-Ramírez, J. Towards a Sustainable Manufacture of Hierarchical Zeolites. *ChemSusChem* **2014**, *7*, 753–764. [CrossRef] [PubMed]
16. Nuttens, N.; Verboekend, D.; Deneyer, A.; Van Aelst, J.; Sels, B.F. Potential of Sustainable Hierarchical Zeolites in the Valorization of α-Pinene. *ChemSusChem* **2015**, *8*, 1197–1205. [CrossRef] [PubMed]
17. Zhang, H.; Hu, Z.; Huang, L.; Zhang, H.; Song, K.; Wang, L.; Shi, Z.; Ma, J.; Zhuang, Y.; Shen, W. Dehydration of Glycerol to Acrolein over Hierarchical ZSM-5 Zeolites: Effects of Mesoporosity and Acidity. *ACS Catal.* **2015**, *5*, 2548–2558. [CrossRef]
18. Groen, J.C.; Jansen, J.C.; Moulijn, J.A.; Pérez-Ramírez, J. Optimal Aluminum-Assisted Mesoporosity Development in MFI Zeolites by Desilication. *J. Phys. Chem. B* **2004**, *108*, 13062–13065. [CrossRef]
19. Suzuki, K.; Aoyagi, Y.; Katada, N.; Choi, M.; Ryoo, R.; Niwa, M. Acidity and Catalytic Activity of Mesoporous ZSM-5 in Comparison with Zeolite ZSM-5, Al-MCM-41 and Silica-Alumina. *Catal. Today* **2008**, *132*, 38–45. [CrossRef]
20. Louis, B.; Ocampo, F.; Yun, H.S.; Tessonnier, J.P.; Pereira, M.M. Hierarchical Pore ZSM-5 Zeolite Structures: From Micro- to Macro-Engineering of Structured Catalysts. *Chem. Eng. J.* **2010**, *161*, 397–402. [CrossRef]
21. Yoo, W.C.; Zhang, X.; Tsapatsis, M.; Stein, A. Synthesis of Mesoporous ZSM-5 Zeolites through Desilication and Re-Assembly Processes. *Microporous Mesoporous Mater.* **2012**, *149*, 147–157. [CrossRef]
22. Ivanova, I.I.; Knyazeva, E.E. Micro-Mesoporous Materials Obtained by Zeolite Recrystallization: Synthesis, Characterization and Catalytic Applications. *Chem. Soc. Rev.* **2013**, *42*, 3671–3688. [CrossRef] [PubMed]
23. Milina, M.; Mitchell, S.; Michels, N.L.; Kenvin, J.; Pérez-Ramírez, J. Interdependence between Porosity, Acidity, and Catalytic Performance in Hierarchical ZSM-5 Zeolites Prepared by Post-Synthetic Modification. *J. Catal.* **2013**, *308*, 398–407. [CrossRef]
24. Zhao, J.; Wang, G.; Qin, L.; Li, H.; Chen, Y.; Liu, B. Synthesis and Catalytic Cracking Performance of Mesoporous Zeolite Y. *Catal. Commun.* **2016**, *73*, 98–102. [CrossRef]
25. Zhang, W.; Ming, W.; Hu, S.; Qin, B.; Ma, J.; Li, R. A Feasible One-Step Synthesis of Hierarchical Zeolite Beta with Uniform Nanocrystals via CTAB. *Materials* **2018**, *11*, 651. [CrossRef] [PubMed]
26. Gueudré, L.; Milina, M.; Mitchell, S.; Pérez-Ramírez, J. Superior Mass Transfer Properties of Technical Zeolite Bodies with Hierarchical Porosity. *Adv. Funct. Mater.* **2014**, *24*, 209–219. [CrossRef]
27. Michels, N.L.; Mitchell, S.; Milina, M.; Kunze, K.; Krumeich, F.; Marone, F.; Erdmann, M.; Marti, N.; Pérez-Ramírez, J. Hierarchically Structured Zeolite Bodies: Assembling Micro-, Meso-, and Macroporosity Levels in Complex Materials with Enhanced Properties. *Adv. Funct. Mater.* **2012**, *22*, 2509–2518. [CrossRef]

28. Michels, N.L.; Mitchell, S.; Pérez-Ramírez, J. Effects of Binders on the Performance of Shaped Hierarchical MFI Zeolites in Methanol-to-Hydrocarbons. *ACS Catal.* **2014**, *4*, 2409–2417. [CrossRef]
29. Suppiah, S. Supported High Silica Zeolites. U.S. Patent 5,157,005, 20 October 1992.
30. Abe, F.; Noda, K. Heater and Catalytic Converter. U.S. Patent 5,538,698, 23 July 1996.
31. Dessau, R.M.; Grasselli, R.K.; Lago, R.M. Processes for Converting Feedstock Organic Compounds. U.S. Patent 5,316,661, 31 May 1994.
32. Grasselli, R.K.; Lago, R.M.; Socha, R.F.; Tsikoyiannis, J.G. NOx Abatement Process. U.S. Patent 5,374,410, 20 December 1994.
33. Zamaro, J.M.; Ulla, M.A.; Miró, E.E. Zeolite Washcoating onto Cordierite Honeycomb Reactors for Environmental Applications. *Chem. Eng. J.* **2005**, *106*, 25–33. [CrossRef]
34. Buciuman, F.C.; Kraushaar-Czarnetzki, B. Preparation and Characterization of Ceramic Foam Supported Nanocrystalline Zeolite Catalysts. *Catal. Today* **2001**, *69*, 337–342. [CrossRef]
35. Ivanova, S.; Louis, B.; Madani, B.; Tessonnier, J.P.; Ledoux, M.J.; Pham-Huu, C. ZSM-5 Coatings on β-SiC Monoliths: Possible New Structured Catalyst for the Methanol-to-Olefins Process. *J. Phys. Chem. C* **2007**, *111*, 4368–4374. [CrossRef]
36. Mitra, B.; Kunzru, D. Washcoating of Different Zeolites on Cordierite Monoliths. *J. Am. Ceram. Soc.* **2008**, *91*, 64–70. [CrossRef]
37. Haden, W.L.; Metuchen, J.; Dzierzanowski, F.J. Method for Making Synthetic Zeolitic Material. U.S. Patent 2,992,068, 11 July 1961.
38. Taggart, E.; Ribaud, G. Process for Producing Molecular Sieve Bodies. U.S. Patent 3,119,659, 28 January 1964.
39. Shimizu, S.; Kiyozumi, Y.; Maeda, K.; Mizukami, F.; Pál-Borbély, G.; Magdolna Mihályi, R.; Beyer, H.K. Transformation of Intercalated Layered Silicates to Zeolites in the Solid State. *Adv. Mater.* **1996**, *8*, 759–762. [CrossRef]
40. Kiricsi, I.; Shimizu, S.; Kiyozumi, Y.; Toba, M.; Niwa, S.I.; Mizukami, F. Catalytic Activity of a Zeolite Disc Synthesized through Solid-State Reactions. *Microporous Mesoporous Mater.* **1998**, *21*, 453–459. [CrossRef]
41. Rao, P.H.P.; Ueyama, K.; Matsukata, M. Crystallization of High Silica BEA by Dry Gel Conversion. *Appl. Catal. A* **1998**, *166*, 97–103.
42. Tosheva, L.; Valtchev, V.; Sterte, J. Silicalite-1 Containing Microspheres Prepared Using Shape-Directing Macro-Templates. *Microporous Mesoporous Mater.* **2000**, *35–36*, 621–629. [CrossRef]
43. You, Z.; Liu, G.; Wang, L.; Zhang, X. Binderless Nano-HZSM-5 Zeolite Coatings Prepared through Combining Washcoating and Dry-Gel Conversion (DGC) Methods. *Microporous Mesoporous Mater.* **2013**, *170*, 235–242. [CrossRef]
44. Mańko, M.; Vittenet, J.; Rodriguez, J.; Cot, D.; Mendret, J.; Brosillon, S.; Makowski, W.; Galarneau, A. Synthesis of Binderless Zeolite Aggregates (SOD, LTA, FAU) Beads of 10, 70 Mm and 1 Mm by Direct Pseudomorphic Transformation. *Microporous Mesoporous Mater.* **2013**, *176*, 145–154. [CrossRef]
45. Yue, M.B.; Yang, N.; Jiao, W.Q.; Wang, Y.M.; He, M.Y. Dry-Gel Synthesis of Shaped Binderless Zeolites Composed of Nanosized ZSM-5. *Solid State Sci.* **2013**, *20*, 1–7. [CrossRef]
46. Fakin, T.; Ristić, A.; Mavrodinova, V.; Zabukovec Logar, N. Highly Crystalline Binder-Free ZSM-5 Granules Preparation. *Microporous Mesoporous Mater.* **2015**, *213*, 108–117. [CrossRef]
47. Bingre, R.; Vincent, B.; Wang, Q.; Nguyen, P.; Louis, B. Assessment of the Improvement of Effective Diffusivity over Technical Zeolite Bodies by Different Techniques. *J. Phys. Chem. C* **2019**, *123*, 637–643. [CrossRef]
48. Fulvio, P.F.; Brosey, R.I.; Jaroniec, M. Synthesis of Mesoporous Alumina from Boehmite in the Presence of Triblock Copolymer. *ACS Appl. Mater. Interfaces* **2010**, *2*, 588–593. [CrossRef] [PubMed]
49. Bleta, R.; Alphonse, P.; Pin, L.; Gressier, M.; Menu, M.-J. An Efficient Route to Aqueous Phase Synthesis of Nanocrystalline γ-Al_2O_3 with High Porosity: From Stable Boehmite Colloids to Large Pore Mesoporous Alumina. *J. Colloid Interface Sci.* **2012**, *367*, 120–128. [CrossRef]
50. Cardoso, C.S.; Licea, Y.E.; Huang, X.; Willinger, M.; Louis, B.; Pereira, M.M. Improving Textural Properties of γ-Alumina by Using Second Generation Biomass in Conventional Hydrothermal Method. *Microporous Mesoporous Mater.* **2015**, *207*, 134–141. [CrossRef]
51. Liu, Q.; Wang, A.; Wang, X.; Gao, P.; Wang, X.; Zhang, T. Synthesis, Characterization and Catalytic Applications of Mesoporous γ-Alumina from Boehmite Sol. *Microporous Mesoporous Mater.* **2008**, *111*, 323–333. [CrossRef]

52. Ertl, G.; Knözinger, H.; Schüth, F.; Weitkamp, J. Physical Properties—Determination of Surface Area. In *Handbook of Heterogeneous Catalysis*, 2nd ed.; Wiley VCH: Weinheim, Germany, 2009; Volume 1, pp. 723–726.
53. Hidalgo, C.V.; Itoh, H.; Hattori, T.; Niwa, M.; Murakami, Y. Measurement of the Acidity of Various Zeolites by Desorption of Ammonia. *J. Catal.* **1984**, *85*, 362–369. [CrossRef]
54. Katada, N.; Igi, H.; Kim, J.-H. Determination of the Acidic Properties of Zeolite by Theoretical Analysis of Temperature-Programmed Desorption of Ammonia Based on Adsorption Equilibrium. *J. Phys. Chem. B* **1997**, *101*, 5969–5977. [CrossRef]
55. Zholobenko, V.L.; Makarova, M.A.; Dwyer, J. Inhomogeneity of Bronsted Acid Sites in H-Mordenite. *J. Phys. Chem.* **1993**, *97*, 5962–5964. [CrossRef]
56. Flego, C.; Kiricsi, I.; Perego, C.; Bellussi, G. The Origin of the Band at 1462 cm-1 Generally Appearing upon Desorption of Pyridine from Acidic Solids. Steps towards a More Comprehensive Understanding. *Catal. Lett.* **1995**, *35*, 125–133. [CrossRef]